Inorganic Chemistry

ARTICLE

pubs.acs.org/IC

Pressure-Induced Local Structure Distortions in $Cu(pyz)F_2(H_2O)_2$

J. L. Musfeldt,*,† Z. Liu,‡ S. Li,§ J. Kang,∥ C. Lee,∥ P. Jena,§ J. L. Manson,⊥ J. A. Schlueter,# G. L. Carr,& and M.-H. Whangbo∥

†Department of Chemistry, University of Tennessee, Knoxville, Tennessee 37996, United States

‡Geophysical Laboratory, Carnegie Institution of Washington, Washington, D.C. 20015, United States

§Department of Physics, Virginia Commonwealth University, Richmond, Virginia 23284, United States

∥Department of Chemistry, North Carolina State University, Raleigh, North Carolina 27695, United States

⊥Department of Chemistry, and Biochemistry, Eastern Washington University, Cheney, Washington 99004, United States

#Materials Science Division, Argonne National Laboratory, Argonne, Illinois 60439, United States

&National Synchrotron Light Source, Brookhaven National Laboratory, Upton, New York 11973, United States

ABSTRACT: We employed infrared spectroscopy along with complementary lattice dynamics and spin density calculations to investigate pressure-driven local structure distortions in the copper coordination polymer $Cu(pyz)F_2(H_2O)_2$. Here, pyz is pyrazine. Our study reveals rich and fully reversible local lattice distortions that buckle the pyrazine ring, disrupt the *bc*-plane O−H···F hydrogen-bonding network, and reinforce magnetic property switching. The resiliency of the soft organic ring is a major factor in the stability of this material. Interestingly, the collective character of the lattice vibrations masks direct information on the Cu−N and Cu−O linkages through the series of pressure-induced Jahn−Teller axis switching transitions, although Cu−F bond softening is clearly identified above 3 GPa. These findings illustrate the importance of combined bulk and local probe techniques for microscopic structure determination in complex materials.

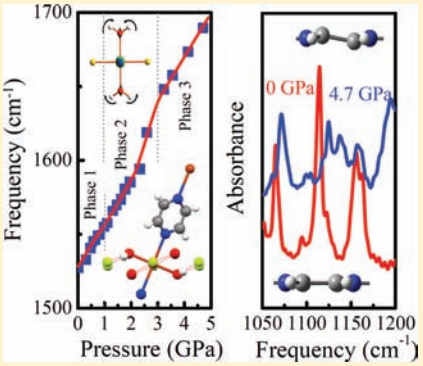

INTRODUCTION

The interplay between charge, structure, and magnetism gives rise to rich behavior in complex materials. External stimuli such as pressure, temperature, or magnetic field can change the balance between interactions and drive new functionality.[1−9] Molecule-based materials offer important advantages over bulk solids for work on pressure-driven transitions because it is relatively easy to modify bond lengths and angles since interatomic potentials are soft and the modulus is low.[10,12−18] As a result, structural distortions take place at only a few GPa rather than under extreme conditions of 50 GPa or more.

$Cu(pyz)F_2(H_2O)_2$ attracted our attention in this regard (Figure 1a).[19−22] Like other coordination polymers, this system is of fundamental interest for studies of quantum magnetism, hydrogen bonding, tunable spin exchange pathways, and magnetic quantum critical transitions.[23−29] Moreover, it displays a series of pressure-driven transitions at room temperature that emanate from sequential Jahn−Teller axis switching.[22] This mechanism depends upon (i) the presence of three different pairs of ligands in trans arrangement around the Cu^{2+} center (Figure 1b) and (ii) distortion of the Cu^{2+} environment in different ways depending upon applied pressure.[22] Recent X-ray work shows that the Jahn−Teller axis is along the N−Cu−N linkage at ambient pressure,[21] switches to the O−Cu−O linkage above 1 GPa,[22] and switches again to the F−Cu−F linkage above 3.3 GPa.[22] Changes in the transition metal coordination sphere thus define three regimes: 0−1 GPa (Phase 1), 1−3.3 GPa (Phase 2), and >3.3 GPa (Phase 3). A two- to one-dimensional magnetic crossover is observed between phases 1 and 2.[22] $Cu(pyz)F_2(H_2O)_2$ is thus an excellent system with which to probe the pressure-dependent interplay between structure and magnetism.

To further test the microscopic aspects of these processes, we measured the infrared vibrational properties of $Cu(pyz)F_2(H_2O)_2$ as a function of pressure using diamond anvil cell techniques and combined our spectral results with complementary lattice dynamics calculations and an analysis of magnetic orbital interactions. We discovered two new pressure-driven local lattice distortions that are large and fully reversible upon release of pressure. The first buckles the pyrazine ligand, whereas the second breaks down two-dimensional hydrogen-bonding ineractions and reinforces the orbitally driven magnetic property switching. Both findings are different from but complementary to the previous crystallographic analysis[22] and are important for establishing structure−function relations in this material. The resiliency of the soft organic ring is a major factor in the stability of $Cu(pyz)F_2(H_2O)_2$ under pressure.

MATERIALS AND METHODS

Single crystals of $Cu(pyz)F_2(H_2O)_2$ were grown as described previously.[19,21] The crystals were crushed and loaded into a symmetric

Received: April 19, 2011
Published: June 06, 2011

   dx.doi.org/10.1021/ic2008039 | *Inorg. Chem.* 2011, 50, 6347–6352

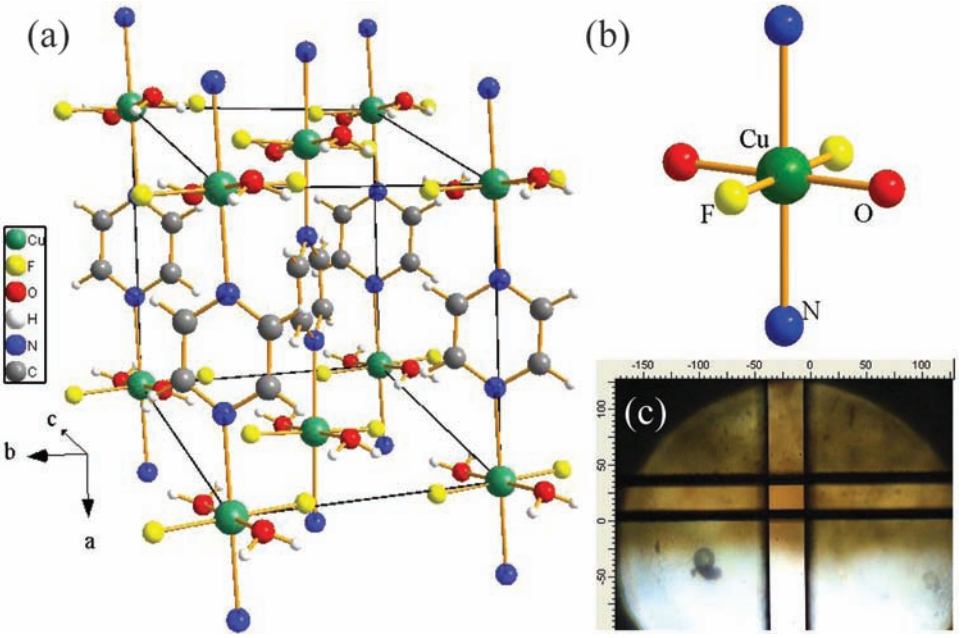

Figure 1. (a) Three nundred Kelvin crystal structure of quasi-one-dimensional $Cu(pyz)F_2(H_2O)_2$ at ambient pressure.[19] (b) Local environment around the Cu^{2+} center at room temperature and ambient pressure. (c) Photograph of the sample and KBr reference inside the diamond anvil cell along with the knife edge aperture positioned to show the measured sample area and a ruby bead for pressure calibration.

diamond anvil cell along with an appropriate pressure medium (vacuum grease or KBr for the far and middle infrared, respectively) and a few ruby balls (Figure 1c). Fluorescence from the latter was used to determine pressure. Our variable-pressure infrared measurements employed the U2A beamline facilities at the National Synchrotron Light Source, Brookhaven National Laboratory. Major instrumentation includes a Bruker Fourier transform infrared spectrometer and microscope attachment, a fluorescence microscope for pressure calculation, and a bolometer detector for added sensitivity in the far-infrared. The high-brightness synchrotron source was essential to overcome throughput limitations imposed by the 500 μm diamond culets and diffraction effects in the far-infrared.[30] For lattice relaxation and dynamical calculations, we employed the projector-augmented wave (PAW) method[31] implemented in the Vienna ab initio simulation package (VASP, version 5.2).[32] The PW91 exchange-correlation functional parametrized by Perdew and Wang was employed in all calculations.[33] We used the Γ-centered $4 \times 4 \times 4$ k mesh and an energy cutoff of 1000 eV. In all calculations, self-consistency was achieved with a tolerance in the total energy of 1×10^{-4} eV. The vibrational frequencies were obtained by diagonalizing the Hessian matrix. For the latter, only symmetry inequivalent displacements were considered, and the remainder of the matrix was filled using symmetry considerations. The spin density was also calculated for the antiferromagnetic state of phase 1 to examine the cause of the pressure-induced magnetic dimensionality crossover.

RESULTS AND DISCUSSION

Figure 2a displays the far-infrared response of $Cu(pyz)F_2(H_2O)_2$ as a function of pressure. The peaks were assigned based upon symmetry analysis, dynamics calculations on the extended lattice as well as on model clusters such as CuF_6^{4-}, and comparison with chemically similar model compounds (Table 1).[20] We assign the peaks below 350 cm^{-1} as Cu−pyrazine-related modes, superimposed in certain cases with Cu−F bending or rocking motion. In most cases, the Cu−pyrazine motion is also combined with very slight twisting, wagging, or rocking of H_2O. Figure 2e shows a representative displacement pattern. The spectral features between 425 and 525 cm^{-1} are assigned as a superposition of out-of-plane pyrazine ring distortion and Cu−F stretching motion. Importantly, all Cu−pyrazine-related lattice and bending modes harden gradually with pressure (Figure 2b). No sharp discontinuities that might correlate with Cu−N contraction at the 1 GPa phase 1 → phase 2 transition are observed.[34] This is because the collective character of the vibrational modes (Table 1) conceals simple changes to the Cu^{2+} coordination sphere. As a result, the normal modes of $Cu(pyz)F_2(H_2O)_2$ do not reveal very much about the softening or hardening of Cu−N and Cu−O bonds through the series of Jahn−Teller transitions. Our discussion therefore focuses on the ligand behavior that is very clearly evidenced by the vibrational properties.

Figure 2c displays a close-up view of the middle-infrared response of $Cu(pyz)F_2(H_2O)_2$ as a function of pressure. The cluster centered at ~1410 cm^{-1} is assigned as in-plane pyrazine ring stretching. We attribute pressure-induced changes in this feature largely to the N−C bonds because the C═C linkage is stiffer by comparison. The broader, weaker structure centered near 1530 cm^{-1} at ambient pressure is assigned as an in-plane, out-of-phase H_2O bending mode in which O is linked to a Cu center (Figure 2f).[20,35] It is red shifted from the characteristic position of coordinated water (between 1600 and 1650 cm^{-1})[36,37] due to substantial distortion and bc-plane H···F hydrogen bonding.[20] This mode hardens by more than 150 cm^{-1} over the 5 GPa pressure range of interest here, with especially strong effects through the 3.3 GPa transition (Figure 2d). As shown in Figures 2 and 3, the deformation, bending, and stretching modes of pyrazine are also very sensitive to pressure, a finding that points to important ring distortions. This is different from the previous crystallographic analysis[22] where pyrazine was assumed to be rigid.[38]

We analyzed the infrared vibrational properties of $Cu(pyz)F_2(H_2O)_2$ to reveal the local lattice distortions in each phase

dx.doi.org/10.1021/ic2008039 |*Inorg. Chem.* 2011, 50, 6347–6352

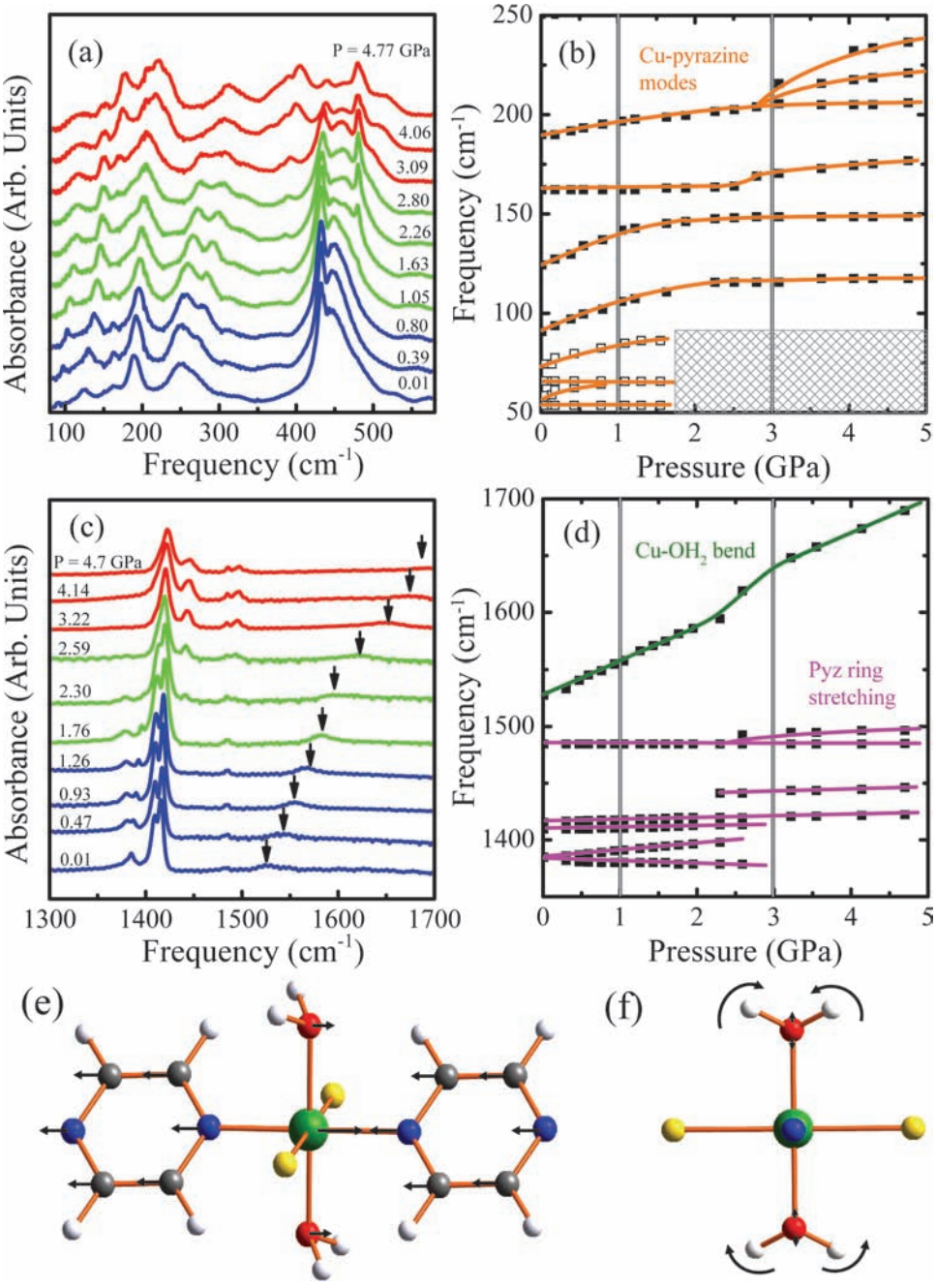

Figure 2. (a) Close-up view of the 300 K absorbance of $Cu(pyz)F_2(H_2O)_2$ in the far-infrared spectral range as a function of pressure. (b) Frequency vs pressure plot of this data. Open symbols denote data from a separate high concentration run where it was not possible to measure above 1.5 GPa. The gray textured area corresponds to this unexplored phase space. Gray vertical lines denote transition pressures. (c) Close up view of the middle infrared absorbance as a function of applied pressure. (d) Frequency vs pressure plot in this regime. Error bars are less than the symbol size. Thin solid lines guide the eye. (e) Calculated displacement pattern for a typical (275 cm^{-1}) Cu-pyrazine lattice mode. (f) Calculated displacement pattern for the (1607 cm^{-1}) $Cu-OH_2$ bend.

making use of the spectral data in Figures 2 and 3 and the mode assignments and calculated displacement patterns summarized in Table 1. Taken together, the behavior of the ring-related modes between 350 and 500 cm^{-1}, near 800 cm^{-1}, at ~985 cm^{-1}, and between 1110 and 1160 cm^{-1} indicates that pyrazine holds up fairly well through the 1 GPa transition, although this soft organic ligand is slightly squashed along *a* and shows a tendency toward both in- and out-of-plane distortion which presumably works to accommodate the reduced cell volume. We attribute the strong blue shift in the 1530 cm^{-1} water bending mode to severe molecular distortion and weakening of the O—H···F hydrogen-bonding network with increasing pressure. Analysis of *b*-directed behavior is more complicated because the Cu—F stretching mode is superimposed upon the out-of-plane N deformation of the pyrazine ring (Table 1). Our data reveal new peaks in the 350—500 cm^{-1} cluster with increasing pressure (Figure 2a). The low-frequency peak at ~370 cm^{-1} in phase 2 is of particular interest because it does not appear in the spectral response of other copper

dx.doi.org/10.1021/ic2008039 |*Inorg. Chem.* 2011, 50, 6347–6352

Table 1. Comparison of Observed Peak Positions in the Infrared Spectrum of $Cu(pyz)F_2(H_2O)_2$ at Ambient Conditions with Predicted Resonance Frequencies from First Principles Dynamics Calculations[a]

observed peak position (cm^{-1}) and strength	calculated frequency (cm^{-1})	description displacement pattern
69.2 (vw)	67.6	pyrazine−Cu−pyrazine rocking
75 (vw)	71.6	pyrazine ring + Cu−F rocking
90.6 (w)	95.5	pyrazine ring rocking
119.6 (w/m)	120.6	pyrazine−Cu−pyrazine bend
161.3 (w)	156	N−Cu−N bend + some F motion
186.2 w/194 shoulder (m)	182, 210	superimposed pyrazine−Cu−pyrazine and F−Cu−F bend
246.9 w/267 shoulder (m)	275 (×2)	pyrazine−Cu−pyrazine asymmetric stretch
432.4, 449.9(m/s)	449, 454, 472 (×2)	out-of-plane N deformation in pyrazine + Cu−F stretch
796.8, 818 doublet (m/m)	796	C−H out-of-plane bend of pyrazine
984.5 (m)	988	C−N−C out-of-plane bending in ring (modulating Cu−N)
1065 (s)	1031	N motion modulating Cu−N distance and C−N−C angles in pyrazine ring
1095.8, 1114.5, 1126.7 triplet (w/s/w)	1104, 1107	in-plane pyrazine stretching
1155.6, 1161.4 doublet (m/m)	1134 1137	in-plane pyrazine stretching (N−C stretch)
1384, 1409.7, 1416.1, 1484.9 (vw/s/s/vw)	1418, 1419, 1486, 1487	in-plane pyrazine stretching (out-of-phase C=C and in-plane N−C stretch)
1523.5 (w)	1607	in-plane, out-of-phase H_2O bend
2921 (vw)	2917	asymmetric H_2O stretch
2965.9, 2986.5, 3005.8, 3041.8, 3055.9 (w)	3102, 3103, 3176 (×2)	various C−H stretching modes
3200−3630 (vs, broad)	3543, 3840	symmetric and asymmetric O−H stretch

[a] Analysis of the calculated displacement patterns combined with a literature review were used to briefly describe the vibrational motion. Most of the low-frequency Cu−pyrazine lattice modes also contain some H_2O twisting, wagging, or rocking character. Peak strength is indicated as vs = very strong, s = strong, m = medium, w = weak, and vw = very weak.

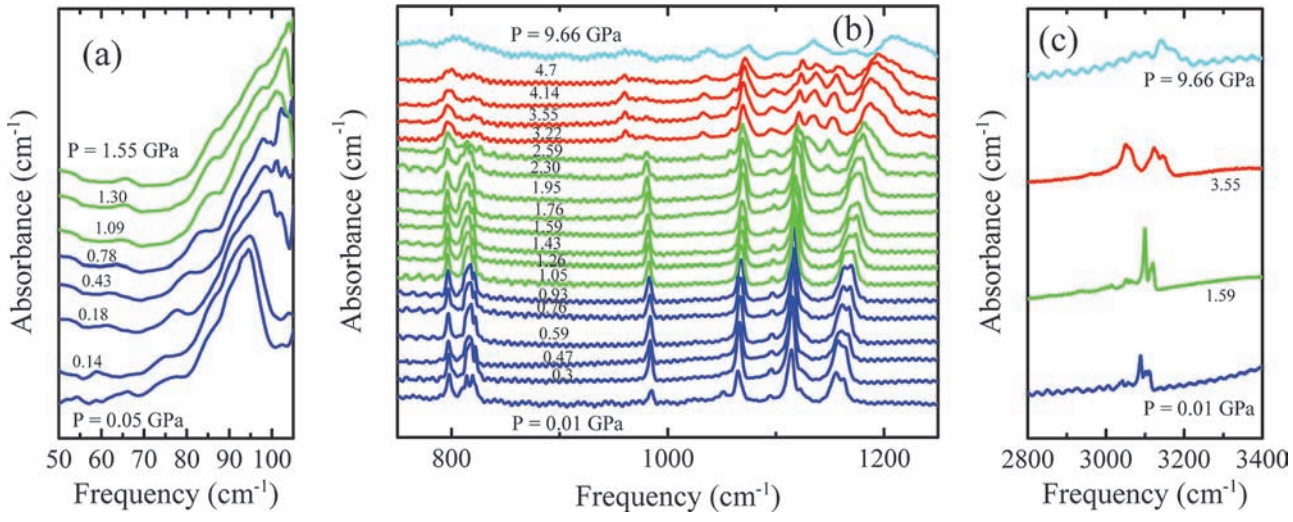

Figure 3. (a) Close-up view of the absorbance of $Cu(pyz)F_2(H_2O)_2$ in the very far-infrared as a function of pressure at 300 K. (b) Middle-infrared vibrational properties as a function of pressure. (c) Close-up view of the C−H stretching regime as a function of applied pressure at room temperature. The peak assignments are listed in Table 1, and the pressure-dependent trends are discussed in the text.

coordination polymers (either under ambient conditions or when the pyrazine ring is clearly distorted).[26,29] We therefore attribute this low-frequency structure to a relaxation of one component of the Cu−F stretching mode. This relaxation is consistent with cell parameter modifications[22] that indicate overall *b*-axis expansion with pressure.[39] Such an expansion weakens the O−H···F hydrogen-bonding network in this material and reinforces the orbital orientation effects that drive the magnetic dimensionality crossover. Increasing the angle of the monoclinic unit cell, β,[11,22] also signals that the Cu−pyrazine chains become less well aligned with increasing pressure and eventually slip past each other, consistent with our observation of hydrogen-bond disruption.

Spectral changes through the 3.3 GPa transition are more dramatic. The most striking is the $Cu-OH_2$ bending mode behavior (Figure 2 (c,d)). This feature hardens strongly through the phase 2 → phase 3 transition. This trend is consistent with compression along the *c* axis and can be considered as an extension of the hydrogen-bonding effects that contribute to

dx.doi.org/10.1021/ic2008039 |*Inorg. Chem.* 2011, 50, 6347–6352

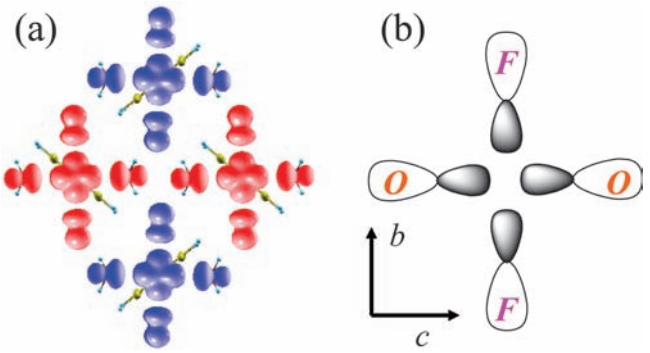

Figure 4. (a) Close-up view of the calculated spin density of Cu(pyz)$F_2(H_2O)_2$ in the *bc* plane. (b) Schematic view of the overlap between the O 2p and F 2p orbitals, associated with a region of four O−H···F hydrogen bonds, leading to two-dimensional magnetic behavior at ambient pressure.

the phase 1 → phase 2 magnetic dimensionality crossover. Here, the coordinated water bending mode shifts from ∼1530 cm^{-1} toward its more commonly observed range (1600−1650 cm^{-1}) when released from OH···F hydrogen-bonding interactions.[20,40] These trends demonstrate the important role of the *bc*-plane hydrogen-bonding networks in Cu(pyz)$F_2(H_2O)_2$ and their severe disruption under pressure. Through the phase 2 → phase 3 transition, reduction of the *c* axis[22] is expected to influence Cu−F stretching mode behavior, although superposition with out-of-plane ring bending motion makes such changes difficult to discern. One signature of this effect and the reduced Cu−F bond length in phase 3 might be the systematic development of the 370 cm^{-1} peak above 3 GPa.[41] The behavior of the ring-related vibrational modes is also quite striking. Specifically, we find (i) symmetry breaking of the superimposed pyrazine−Cu−pyrazine + F−Cu−F bending mode at 185 cm^{-1}, (ii) a strong change in the position and shape of the out-of-plane pyrazine bending modes (between 350 and 500, near 800, and at 985 cm^{-1}), (iii) a systematic blue shift, broadening, and strong symmetry breaking of the in-plane pyrazine stretching modes between 1050 and 1200 cm^{-1}, and (iv) a C−H stretching signature near 3100 cm^{-1} that is significantly broadened and shifted compared with that in the ambient-pressure phase. Taken together, these changes point toward a major local symmetry reduction through the 3.3 GPa transition that involves both in-plane and out-of-plane distortions. We attribute these effects to pyrazine ring buckling.

Although our work focuses on the transitions between phases 1, 2, and 3, we are also interested in the properties of Cu(pyz)$F_2(H_2O)_2$ above 5 GPa. Figure 3 displays data taken at 9.66 GPa in several important frequency ranges. The diffuse spectral character is indicative of a grossly distorted, low-symmetry phase. Interestingly, all pressure-induced spectral changes are fully reversible upon release of pressure, a characteristic that we attribute to the resiliency of the soft organic ring.

Finally, we examine how the two-dimensional antiferromagnetism of phase 1 changes to one-dimensional antiferromagnetism in phase 2 under pressure. The spin density plot calculated for the antiferromagnetic state of phase 1 shows the expected features (Figure 4a). The $x^2 - y^2$ magnetic orbital on each Cu^{2+} site makes σ-antibonding interactions with the p orbitals of its first-coordinate ligand atoms (i.e., the two O and two F centers).[42] Every four adjacent Cu^{2+} sites are arranged such that the two O centers and the two F atoms make an O_2F_2 rhombus with the O···O diagonal shorter than the F···F diagonal, in which the O 2p and F 2p orbitals run along the O···O and F···F diagonals, respectively. The two-dimensional magnetic character of phase 1 thus arises from the overlap between two adjacent, orthogonally oriented, 2p orbitals in each O_2F_2 rhombus (Figure 4). As the Jahn−Teller axis switches from N−Cu−N to O−Cu−O to F−Cu−F,[22] the magnetic orbital plane changes from CuO_2F_2 to CuN_2F_2 to CuN_2O_2. Consequently, in phases 2 and 3 adjacent magnetic orbitals can overlap only along one direction so that they possess one-dimensional magnetic character. This explains the observed two- to one-dimensional magnetic crossover through the 1 GPa transition.

CONCLUSION

To summarize, there is broad interest in the use of external stimuli to manipulate the properties of complex materials. This work combines diamond anvil cell techniques with ultra-bright synchrotron radiation-based infrared spectroscopy and complementary lattice dynamics and spin density calculations for a microscopic analysis of local structure distortions in Cu(pyz)$F_2(H_2O)_2$ through the series of pressure-induced transitions. Our work reveals that increasing pressure disrupts the *bc*-plane O−H···F hydrogen-bonding network and significantly distorts the pyrazine ring. The ring distortion is small at 1 GPa but becomes substantial above 3 GPa, with significant out-of-plane buckling. The resiliency of the soft organic ring upon release of pressure is a major factor in the stability of this material. The displacement patterns of the low-frequency vibrational modes are highly collective in character, masking direct information about Cu−N and Cu−O bond hardening or softening. Nevertheless, Cu−F bond softening, expected for the phase 2 to 3 transition, is clearly identified. These findings illustrate the importance of combining bulk and local probe techniques for microscopic structure determination in novel materials.

AUTHOR INFORMATION

Corresponding Author
*E-mail: musfeldt@utk.edu.

ACKNOWLEDGMENT

This research was supported by the DoE (UT, BNL, NCSU, VCU, ANL), the NSF (EWU), and the Research Corporation (EWU). We thank P. Chen for technical assistance and D. Schlueter for timely action.

REFERENCES

(1) Goncharov, A. F.; Struzhkin, V. V.; Somayazulu, M. S.; Hemley, R. J.; Mao, H. K. *Science* **1996**, *273*, 218–220.
(2) Iota, V.; Yoo, C. S.; Cynn, H. *Science* **1999**, *283*, 1510–1513.
(3) Hemley, R. J.; Mao, H. K.; Gramsch, S. A. *Miner. Mag.* **2000**, *64*, 157–184.
(4) Yoo, C. S.; Maddox, B.; Klepeis, J.-H. P.; Iota, V.; Evans, W.; McMahan, A.; Hu, M. Y.; Chow, P.; Somayazulu, M.; Häusermann, D.; Scalettar, R. T.; Pickett, W. E. *Phys. Rev. Lett.* **2005**, *94*, 115502.
(5) Gupta, R.; Kim, M.; Barath, H.; Cooper, S. L.; Cao, G. *Phys. Rev. Lett.* **2006**, *96*, 067004.
(6) Chen, X.-J.; Struzhkin, V. V.; Song, Y.; Goncharov, A. F.; Ahart, M.; Liu, Z.; Mao, H.-K.; Hemley, R. J. *Proc. Natl. Acad. Sci.* **2008**, *105*, 20–23.

(7) Imai, T.; Ahilan, K.; Ning, F. L.; McQueen, T. M.; Cava, R. J. *Phys. Rev. Lett.* **2009**, *102*, 177005.
(8) Torikachvili, M. S.; Bud'ko, S. L.; Ni, N.; Canfield, P. C.; Hannahs, S. T. *Phys. Rev. B* **2009**, *80*, 013521.
(9) Cui, H. B.; Graf, D.; Brooks, J. S.; Kobayashi, H. *Phys. Rev. Lett.* **2009**, *102*, 237001.
(10) Bini, R.; Ballerini, R.; Pratesi, G.; Jodl, H. J. *Rev. Sci. Instrum.* **1997**, *68*, 3154–3160.
(11) This angle quantifies Cu−pyrazine chain alignment.
(12) Kawamoto, T.; Tokumoto, M.; Sakamoto, H.; Mizocuchi, K. *Phys. Soc. Jpn.* **2001**, *70*, 1892–1895.
(13) Allen, D. R.; Blake, A. J.; Huang, D.; Prior, T. J.; Schröder, M. *Chem. Commun.* **2006**, 4081–4083.
(14) Pravica, M.; Yulga, B.; Liu, Z.; Tschauner, O. *Phys. Rev. B* **2007**, *76*, 064102.
(15) Dong, Z.; Beulby, N. G.; Huang, Y.; Song, Y. *J. Chem. Phys.* **2008**, *128*, 074501.
(16) Song, Y.; Murli, C.; Liu, Z. *J. Chem. Phys.* **2009**, *131*, 174506.
(17) Murata, K.; Yokogawa, Y.; Brooks, J. S.; Kismarahardja, A.; Steven, E.; Kano, M.; Seno, Y.; Tamilselvan, N. R.; Yoshino, H.; Sasaki, T.; Jerome, D.; Senzier, P.; Bechgaard, K.; Uruichi, M.; Yakushi, K. *J. Phys.: Conf. Series* **2010**, *215*, 012064.
(18) Thirunavukkuarasu, K.; Long, V. C.; Musfeldt, J. L.; Borondics, F.; Klupp, G.; Kamarás, K.; Kuntscher, C. A. *J. Phys. Chem. C* **2011**, *115*, 3646–3653.
(19) Conner, M.; McConnell, A.; Schlueter, J. A.; Manson, J. L. *J. Low Temp. Phys.* **2006**, *142*, 273–278.
(20) Brown, S.; Cao, J.; Musfeldt, J. L.; Conner, M. M.; McConnell, A. C.; Southerland, H. I.; Manson, J. L.; Schlueter, J. A.; Phillips, M. D.; Turnbull, M. M.; Landee, C. P. *Inorg. Chem.* **2007**, *46*, 8577–8583.
(21) Manson, J. L.; Conner, M. M.; Schlueter, J. A.; McConnell, A. C.; Southerland, H. I.; Malfant, I.; Lancaster, T.; Blundell, S. J.; Brooks, M. L.; Pratt, F. L.; Singleton, J.; McDonald, R. D.; Lee, C.; Whangbo, M.-H. *Chem. Mater.* **2008**, *20*, 7408–7416.
(22) Halder, G. J.; Chapman, J. W.; Schlueter, J. A.; Manson, J. L. *Angew. Chem., Int. Ed.* **2011**, *50*, 419–421.
(23) Jones, B. R.; Varughese, P. A.; Pigos, J. M.; Musfeldt, J. L.; Landee, C. P.; Turnbull, M. M.; Olejniczak, I.; Carr, G. L. *Chem. Mater.* **2001**, *13*, 2127–2134.
(24) Goddard, P. A.; Singleton, J.; Sengupta, P.; McDonald, R. D.; Lancaster, T.; Blundell, S. J.; Pratt, F. L.; Cox, S.; Harrison, N.; Mason, J. L.; Southerland, H. I.; Schlueter, J. A. *New J. Phys.* **2008**, *10*, 083025.
(25) Manson, J. L.; Schlueter, J. A.; Funk, K. A.; Southerland, H. I.; Twamley, B.; Lancaster, T.; Blundell, S. J.; Baker, P. J.; Pratt, F. L.; Singleton, J.; McDonald, R. D.; Goddard, P. A.; Sengupta, P.; Batista, C. D.; Ding, L.; Lee, C.; Whangbo, M.-H.; Franke, I.; Cox, S.; Baines, C.; Trial, D. *J. Am. Chem. Soc.* **2009**, *131*, 6733–6747.
(26) Musfeldt, J. L.; Vergara, L. I.; Brinzari, T. V.; Tung, L. C.; Wang, Y. J.; Schlueter, J. A.; Manson, J. L.; Sun, C.; Whangbo, M.-H. *Phys. Rev. Lett.* **2009**, *103*, 157401.
(27) Cizmár, E.; Zvyagin, S. A.; Beyer, R.; Uhlarz, M.; Ozerov, M.; Skourski, Y.; Manson, J. L.; Schlueter, J. A.; Wosnitza, J. *Phys. Rev. B* **2010**, *81*, 064422.
(28) White, J. L.; Lee, C.; Gunaydin-Sen, O.; Tung, L. C.; Christen, H. M.; Wang, Y. J.; Turnbull, M. M.; Landee, C. P.; McDonald, R. D.; Crooker, S. A.; Singleton, J.; Whangbo, M.-H.; Musfeldt, J. L. *Phys. Rev. B* **2010**, *81*, 052407.
(29) Gunaydin-Sen, Ö.; Lee, C.; Tung, L. C.; Chen, P.; Turnbull, M. M.; Landee, C. P.; Wang, Y. J.; Whangbo, M.-H.; Musfeldt, J. L. *Phys. Rev. B* **2010**, *81*, 104307.
(30) Carr, G. L.; Martin, M. C.; McKinney, W. R.; Neil, G. R.; Jordan, K.; Williams, G. P. *Nature* **2002**, *420*, 153–156.
(31) Blöchl, P. E. *Phys. Rev. B* **1994**, *50*, 17953.
(32) Kresse, G.; Furthmüller, J. *Phys. Rev. B* **1996**, *54*, 11169.
(33) Wang, Y.; Perdew, J. P. *Phys. Rev. B* **1991**, *44*, 013298.
(34) There is some additional symmetry breaking above 3 GPa.
(35) This is a fairly isolated H_2O mode, unconnected to the Cu^{2+} coordination sphere.
(36) Nakamoto, K. *Infrared and Raman spectra of inorganic and coordination compounds*, 4th ed.; Wiley: New York, 1986.
(37) Brubach, J.-B.; Mermet, A.; Filabozzi, A.; Gerschel, A.; Roy, P. *J. Chem. Phys.* **2005**, *122*, 184509.
(38) Similar effects are observed in the fully deuterated analog $Cu(d_4\text{-pyz})F_2(D_2O)_2$.
(39) The *b*-axis length decreases gradually with increasing pressure within phases 1, 2 and 3 but increases discontinuously across the phase boundaries.[22]
(40) The agreement between theory and experiment (Table 1) improves with increasing pressure as hydrogen bonding plays a less dominant role.
(41) As with the H_2O bending mode, precursor effects are clearly evident.
(42) Whangbo, M.-H.; Koo, H.-J.; Dai, D. *J. Solid State Chem.* **2003**, *176*, 417–422.